Diffusion-weighted imaging of bone marrow

Olaf Dietrich[1], Andreas Biffar[1], Maximilian F. Reiser[1,2], Andrea Baur-Melnyk[2]

[1] Josef Lissner Laboratory for Biomedical Imaging, Department of Clinical Radiology – Grosshadern, LMU Ludwig Maximilian University of Munich, Munich, Germany

[2] Department of Clinical Radiology – Grosshadern, LMU Ludwig Maximilian University of Munich, Munich, Germany

Semin Musculoskelet Radiol 2009; **13**(2): 134–144 <URL:http://dx.doi.org/10.1055/s-0029-1220884>

Abstract

In diffusion-weighted magnetic resonance imaging (DWI), the observed MRI signal intensity is attenuated by the self-diffusion of water molecules. DWI can provide information about the microscopic structure and organization of biological tissue and, thus, can depict various pathological changes of organs or tissues. DWI has been successfully used for the characterization of bone marrow alterations or lesions, and in particular for the differentiation of benign and malignant vertebral compression fractures. In this review article, the basics of diffusion-weighted magnetic resonance imaging are introduced and several pulse sequences, which have been used for DWI of the bone marrow, are described. Subsequently, an extensive overview about diffusion studies of the bone marrow and in particular of DWI of vertebral compression fractures is given.

Keywords:

Diffusion-weighted magnetic resonance imaging, Bone marrow, Vertebral compression fractures, Pulse sequences

Corresponding author:

Olaf Dietrich, PhD
Josef Lissner Laboratory for Biomedical Imaging
Department of Clinical Radiology – Grosshadern
LMU Ludwig Maximilian University of Munich
Marchioninistr. 15
81377 Munich
Germany
Phone: +49 89 7095-3623
Fax: +49 89 7095-4627
E-mail: od@dtrx.net

Introduction

Diffusion-weighted magnetic resonance imaging (DWI) is an established magnetic resonance imaging (MRI) technique, in which the MRI signal intensity is influenced by the self-diffusion, i.e., the stochastic Brownian motion of water molecules. DWI can provide information about the microscopic structure and organization of biological tissue and, thus, can depict various pathological changes of organs or tissues. It has been thoroughly evaluated for a multitude of neurological pathologies[1] such as brain tumors[2], abscesses[3], or white-matter diseases[4], and in particular for the early detection of cerebral ischemia[5,6], which can be considered the most important application of clinical DWI.

Significantly fewer studies have been published about DWI outside the brain, mainly because of the limited image quality and the relatively low robustness of conventional DWI methods in non-neurological applications. This situation, however, improved in recent years due to better hardware and new pulse sequences, and several new applications of DWI have been described. Many of these are focused on oncological imaging, e.g. of the liver[7,8] or kidneys[9,10] or of soft-tissue tumors[11,12]. Very recently, even whole-body DWI was proposed to improve the detection of malignancies[13,14].

Since the late 1990s, DWI has also been successfully used for the detection and characterization of bone-marrow alterations. The most important clinical application of DWI in bone marrow is the differentiation of benign (e.g. osteoporotic or traumatic) and malignant vertebral compression fractures[15–17]. Unfortunately, DWI of the bone marrow is complicated by the fact that significant variations of susceptibility occur in the anatomical neighborhood of bone structures resulting in severe distortion artifacts when standard echo-planar DWI techniques are applied. Hence, several alternative diffusion-weighting pulse sequences were proposed and evaluated for DWI of the bone marrow[18] as described below.

In this review article, we will first introduce the basics of diffusion-weighted MRI and then describe several specific MRI techniques, which have been used for DWI of bone marrow. Subsequently, we will give an extensive overview about diffusion studies of the bone marrow and in particular of vertebral compression fractures.

Basics

DWI is a magnetic resonance (MR) technique that is sensitive to the Brownian molecular motion of spins. Already in 1950, Erwin Hahn described that the presence of a magnetic field gradient during a spin-echo experiment results in a signal attenuation due to the diffusive motion of the spins[19]. An improved strategy to quantify the diffusion coefficient in a magnetic resonance experiment was proposed in 1965 by Stejskal and Tanner[20]. In their experiment, a pair of additional gradient pulses is inserted into a pulse sequence, the so-called Stejskal-Tanner diffusion gradients.

The effect of these diffusion gradients is to attenuate the transversal magnetization, i.e., the received MR signal intensity, depending on the extent of molecular motion as illustrated in Fig. 1. The first diffusion gradient dephases the spins, i.e., the spins are prepared with a spatially varying additional phase angle. In the case of stationary spins, the additional phase angle is exactly reverted by the second diffusion gradient, resulting in the same transversal magnetization after the second gradient as without diffusion sensitizing. If, however, the spins move stochastically between the two diffusion gradients, then each single spin experiences a different magnetic field at the time of the second gradient pulse than during dephasing. Consequently, the second gradient does not fully revert the dephasing and a certain, stochastically distributed phase angle remains. This random distribution of phase angles is observed as signal attenuation, which is, thus, a measure of molecular diffusion.

The diffusion of molecules in a liquid or gas is physically described by the diffusion coefficient, *D*. The diffusion coefficient is frequently given in units of mm^2/s and describes the mean displacement, *d*, of molecules during a time, τ (usually referred to as diffusion time):

$$d = \sqrt{6 \cdot D \cdot \tau}$$

The diffusion coefficient of pure water at room temperature, for instance, is approximately $2 \times 10^{-3}\,mm^2/s$, resulting in a mean displacement

of about 25 µm in 50 ms. As explained above, the attenuation of the magnetic resonance signal, i.e. the ratio of the measured signal, $S(D, b)$, and the original signal without diffusion gradients, S_0, depends on the diffusion coefficient, D, and on the properties of the diffusion gradients, which are summarized within the so-called diffusion weighting, b, or b-value of the pulse sequence:

$$S(D, b) = S_0 \cdot \exp(-b \cdot D).$$

The b-value of the sequence can be calculated from the properties of the diffusion gradients shown in Fig. 1, i.e. from their amplitude, g_D, their duration, δ, and the interval between their onsets, Δ:

$$b = (\gamma \cdot g_D \cdot \delta)^2 \cdot (\Delta - \delta/3)$$

where γ is the gyromagnetic ratio of the diffusing spins. The b-value is expressed in units of s/mm²; typical values for DWI range from 50 to 1500 s/mm².

The b-value of a pulse sequence plays the same role in DWI as the echo time in T_2-weighted MRI: Higher diffusion weightings increase the contrast between tissues with different diffusion coefficients, but at the same time decrease the overall signal intensity. Hence, the choice of the optimal diffusion weighting is always a compromise between diffusion contrast on the one hand and the signal-to-noise ratio (SNR) on the other hand[21]. In addition, long echo times are required for high diffusion weightings due to the long diffusion gradient pulses and, thus, the SNR of the diffusion-weighted images is further decreased.

Another general problem of DWI is the very high motion sensitivity of diffusion-sensitized pulse sequences[22,23]. Since the diffusion gradients are inserted in order to depict stochastic molecular motions in the range of some 10 micrometers, DWI becomes very sensitive to any macroscopic patient motions as well. Several different approaches were suggested in order to increase the robustness of DWI techniques as described in the following section.

In applications of DWI in vivo, the most important diffusing molecule is water. Generally, water diffusion in tissue is influenced by the properties of the cells, in particular by the cell size and their geometric structure. Typical diffusion coefficients of water measured in vivo are in the range between 0.3 and 3×10^{-3} mm²/s. The diffusion coefficient is decreased compared to free water diffusion due to the presence of cell membranes, cell organelles, or large macromolecules, which restrict and hinder the molecular motion. The actually measured diffusion coefficient in vivo is therefore called "apparent diffusion coefficient" (ADC).

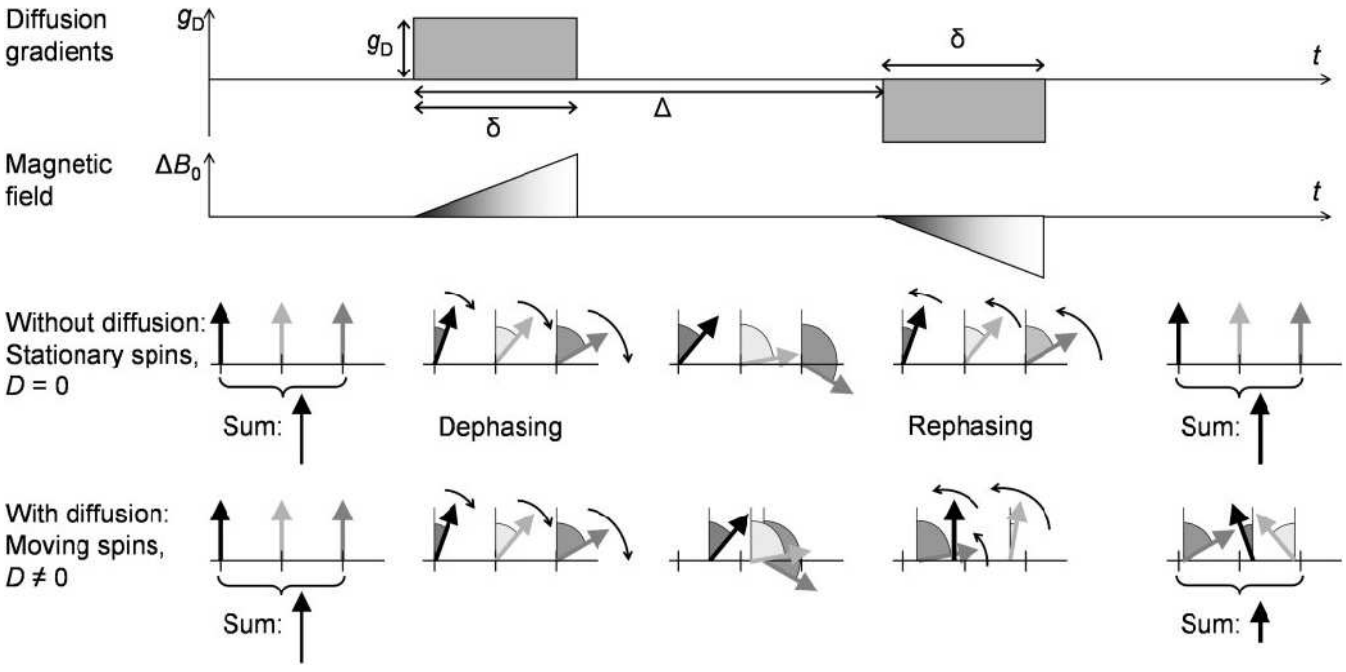

Figure 1: Effect of diffusion gradients. The diffusion gradients (top row) cause a spatially varying magnetic field, B_0, (second row) and, thus, spatially varying Larmor frequencies. The first diffusion gradient dephases the spins (three spins at different spatial positions are shown as grey and black arrows). If the spins are stationary (no diffusion), the second diffusion gradient with opposite sign exactly rephases the spins. In the case of diffusing spins, however, rephasing is incomplete since the spins have moved between the first and the second diffusion gradient; thus, a diffusion-dependent signal attenuation is observed as illustrated by the "sum" arrows.

By applying diffusion gradients in a single spatial direction as illustrated in Fig. 1, only diffusional motion parallel to this direction is detected. While this experiment is sufficient to measure the diffusion properties in e.g. isotropic liquids, the situation in tissue can be much more complex. In particular in highly anisotropic tissues such as nerve or muscle fibers, diffusion will be higher parallel to the fiber direction than perpendicular to it. In this case, diffusion is not longer described by a single diffusion coefficient but by the diffusion tensor, which can be represented by a matrix containing 6 independent values[24,25]. To measure the diffusion tensor, several diffusion measurements (at least 6 corresponding to the number of independent matrix components) are required that can be obtained by applying diffusion gradients in different spatial directions[26].

Techniques

Diffusion-sensitizing gradients can be inserted in many different types of pulse sequences. Historically, DWI was first performed with stimulated-echo and spin-echo pulse sequences (Fig. 2a and 2b)[27–29]. These pulse sequences, however, require very long acquisition times, and, thus, are very prone to motion artifacts. Although different strategies were proposed to reduce their motion sensitivity such as navigator-echo motion correction[30–32], radial k-space sampling[33,34], or line-scan-imaging techniques[35] they are generally not applied in clinical routine applications today.

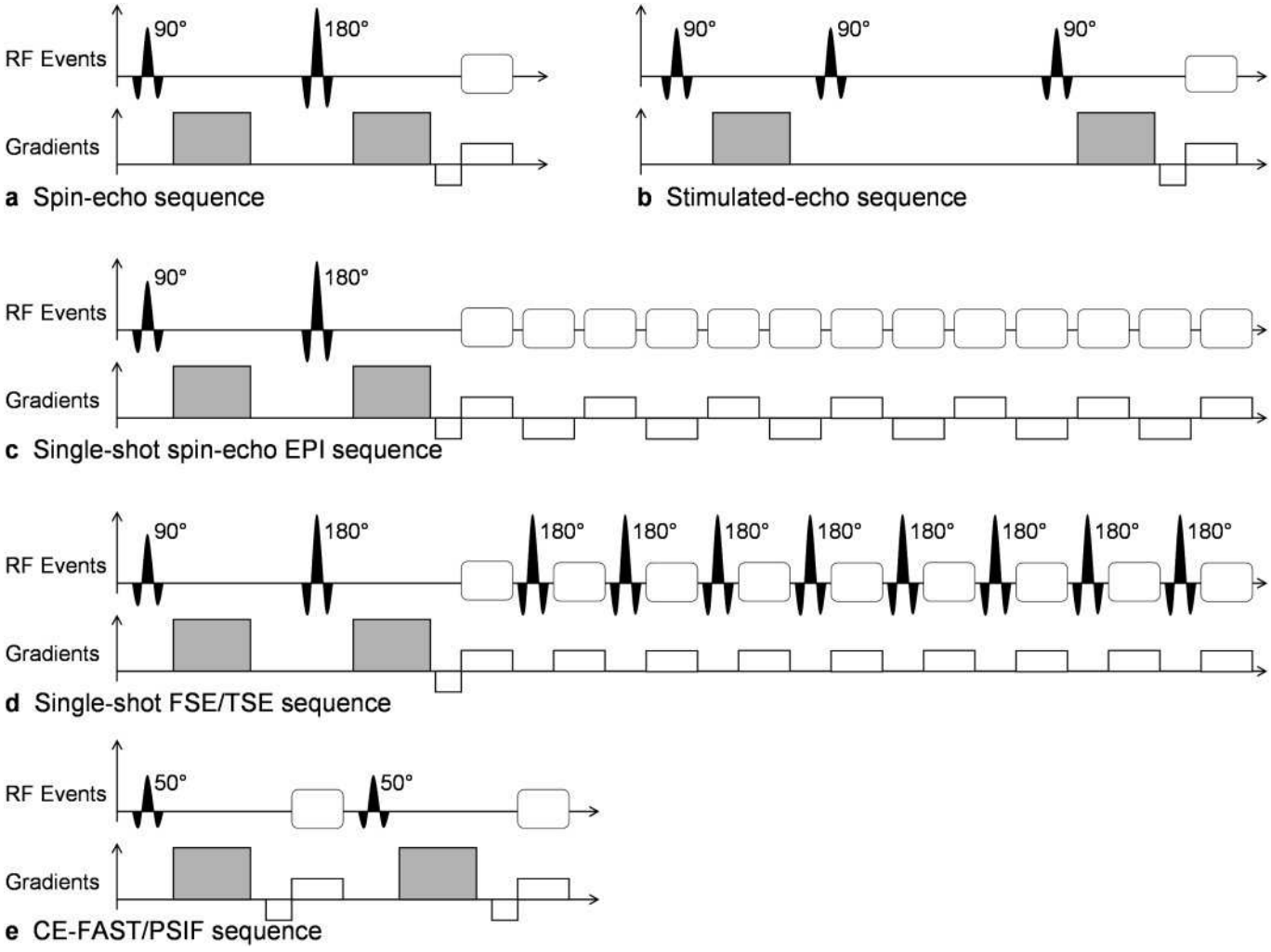

Figure 2: Pulse sequences used for DWI. Sequences are simplified by displaying only the diffusion gradients (gray boxes) and the imaging gradients in readout direction (white boxes). (a, b) a single repetition of a spin-echo and simulated-echo sequence; (c, d): echo trains of single-shot spin-echo echo-planar and fast-spin-echo sequences; (e) two subsequent repetitions of a CE-FAST (PSIF) sequence.

The most important pulse sequence for DWI in general is the single-shot spin-echo echo-planar imaging (EPI) sequence (Fig. 2c)[36]. Because of the very fast readout of the complete image data within about 100 ms, this sequence is relatively insensitive to macroscopic motion. In the presence of susceptibility variations, however, echo-planar images frequently suffer from gross geometrical image distortions due to the long gradient-echo train. This property of EPI is a severe limitation for the application outside the brain where structures or organs of interest are frequently found in the direct neighborhood of air-filled spaces or bone-soft-tissue borders with substantially different susceptibilities. A second disadvantage of single-shot EPI is the relatively low spatial resolution achievable with this approach. The single-shot readout typically limits the spatial resolution to matrix sizes of 128×128. Only relative recent innovations in hardware and acquisition techniques substantially improved the suitability of EPI for non-neuroradiological DWI. Improved gradient systems with reduced eddy-current effects and particularly the application of parallel imaging techniques can reduce geometric distortions and, at the same time, increase the spatial resolution of single-shot EPI acquisitions[37].

A second approach to reduce artifacts and to increase the spatial resolution of EPI acquisitions is a segmented (or multi-shot) echo-planar readout. By shortening the echo train length, the segmented EPI sequence becomes less sensitive to susceptibility variations. However, the total acquisition time is increased and the robustness against motion artifacts is reduced.

An alternative to diffusion-weighted EPI acquisitions are diffusion-weighted single-shot sequences based on the acquisition of spin-echo trains, i.e. single-shot fast-spin-echo or turbo-spin-echo pulse sequences also known as "rapid acquisition with relaxation enhancement" (RARE) or "half-Fourier-acquisition single-shot turbo-spin-echo" (HASTE) sequences (Fig. 2d)[38]. Similarly to echo-planar sequences, these approaches are very fast (200–400 ms per image) and relatively insensitive to motion, but also limited in their spatial resolution. An advantage compared to EPI is the insensitivity to susceptibility variations. However, inserting diffusion gradients into the spin-echo train destroys the originally equal spacing of refocusing RF pulses and, thus, can induce new image artifacts. Several approaches have been suggested to overcome this disadvantage, but most solutions also reduce the signal-to-noise ratio of the acquired images[38–40]; thus, single-shot fast-spin-echo DWI frequently requires the acquisition of multiple averages in order to obtain a sufficient SNR. As for EPI, parallel imaging can be employed to increase the spatial resolution that can be acquired with a single echo train and to reduce some image artifacts such as image blurring in phase-encoding direction.

Some remaining disadvantages of single-shot fast-spin-echo techniques can be overcome by segmenting the readout similarly as in segmented EPI acquisitions. A particularly promising approach is the recently proposed diffusion-weighted PROPELLER (periodically rotated overlapping parallel lines with enhanced reconstruction) MRI sequence[41] or BLADE sequence. With this non-Cartesian technique, k-space is covered by rotated rectangular strips that allow for a robust motion correction due to the oversampled center of k-space, which is included in every single echo train.

A very different approach for DWI (in particular of the spinal column) is the application of steady-state free-precession (SSFP) sequences (Fig. 2e). The SSFP sequence type used for DWI is the diffusion-weighted contrast-enhanced Fourier-acquired steady-state technique (CE-FAST) or PSIF sequence[42,43], where PSIF is the reversed version (with respect to both the acronym and the sequence timing) of the "fast imaging with steady precession" (FISP) sequence. In contrast to the other approaches described above, only a single (monopolar) diffusion gradient is inserted into each repetition time, TR, of the PSIF sequence (Fig. 2e shows two subsequent TRs)[44,45]. Spins dephased by the diffusion-sensitizing gradients are rephased by a second diffusion gradient later in the sequence scheme, however, not necessarily by the immediately subsequent one. Thus, the diffusion time, τ, of the PSIF sequence cannot easily be determined, but depends on the relaxation times, T_1 and T_2, and on the sequence parameters, TE, TR, and the flip angle[46,47]. Although this makes the exact quantification of the ADC very difficult, diffusion-weighted images acquired by the PSIF sequence have been shown to be extremely valuable for the differential diagnosis of vertebral compression fractures[15–17]. The diffusion-weighted PSIF approach is relatively fast due to the short repetition times in the order of

typically 20 to 30 ms. Consequently, the PSIF sequence is also relatively insensitive to the influence of bulk motion. Newer developments of SSFP DWI include the implementation of diffusion-weighted 3D sequences, which have been applied e.g. for DWI of the cartilage[48].

Applications

As mentioned above, one of the most successful applications of diffusion-weighted imaging of the bone marrow is the differentiation of benign osteoporotic and malignant vertebral compression fractures, which has first been demonstrated by Baur et al. in 1998[16]. In this study, the pathological differentiation was based on the relative signal intensity of the affected vertebra in non-quantitative DWI with a diffusion-weighted SSFP sequence. Baur et al. demonstrated that benign osteoporotic fractures appear hypointense or isointense in SSFP-based DWI, while malignant fractures caused by bone-marrow tumors and metastases appear hyperintense. Several similar studies of non-quantitative DWI of vertebral compression fractures are summarized in Table 1. The results of most of these studies are compatible with a general tendency to hypointensity in benign vertebral fractures and to hyperintensity in malignant fractures; image examples are shown in Figs. 3 and 4. Typically, this signal behavior showed up more clearly with the diffusion-weighted SSFP approach than with alternative pulse sequences such as single-shot EPI, single-shot FSE, or conventional spin-echo or stimulated echo sequences (cf. Table 1).

Partially disagreeing results were reported by Castillo et al., who found a number of hypointense vertebral metastases in diffusion-weighted SSFP acquisitions[49]. These results may be explained by the fact that some patients with hypointense metastases were treated with radiotherapy before imaging and some other patients had sclerotic metastases that appear hypointense due to their very low water content. Recently, Hackländer et al. noted that particularly vertebral metastases of prostate cancer show less signal than metastases of other tumors[50]. This result may also explain some of the hypointense signals observed by Castillo et al.

Table 1: Non-quantitative DWI of vertebral bone marrow (v.b.m.)

Study	Pulse sequence[a]	Diffusion weighting (gradient moment or b-values)	# of patients	Signal relative to normal v.b.m.[b]	
				benign (osteoporotic/ traumatic) fracture	malignant fracture or metastasis
Byun et al. 2007[55]	SSFP	120 ms mT/m	22	↓	↑
Hackländer et al. 2006[50]	SSFP	25 ms mT/m	38	–	↑ (↔) [c]
Park et al. 2004[56]	ss-FSE	500 s/mm²	46	↓ (↔)	↓ ↔ (↑)
Abanoz et al. 2003[57]	SSFP	115 ms mT/m	49	↓ ↔	↑ [d]
Baur et al. 2002[58]	SSFP	69 ms mT/m	85	↓ (↔) (↑)	↑
Byun et al. 2002[59]	SSFP	48 ms mT/m	24	–	↑
Yasumoto et al. 2002[60]	ss-EPI	30, 300, 900 s/mm²	53	↓ (↔) (↑) [e]	↑ (↔) (↓) [e]
Spuentrup et al. 2001[61]	SE, STE	0, 360/598 s/mm²	34	↓	↔
Baur et al. 2001[62]	SSFP	138 ms mT/m	29	↓ (↔)	↑
Castillo et al. 2000[49]	SSFP	48 ms mT/m	15	–	↓ ↔ ↑
Baur et al. 1998[16]	SSFP	46 ms mT/m	30	↓ (↔)	↑

[a] Sequences: SSFP: diffusion-weighted steady-state free-precession (or PSIF) sequence; ss-FSE: diffusion-weighted single-shot fast-spin-echo sequence; ss-EPI: diffusion-weighted single-shot spin-echo echo-planar imaging sequence with fat saturation; SE, STE: diffusion-weighted spin-echo or stimulated-echo sequence

[b] ↓: lesion hypointense, ↔: lesion isointense, ↑: lesion hyperintense, parentheses: sporadic observations, –: no data

[c] results for non-prostate-carcinoma metastases; 18 metastatic lesions from prostate carcinoma showed mixed contrasts (hypo-, iso-, or hyperintense)

[d] 3 lesions in inflammatory diseases also hyperintense

[e] results for iliac bone marrow without (left) or with (right) infiltration of malignant lymphoma

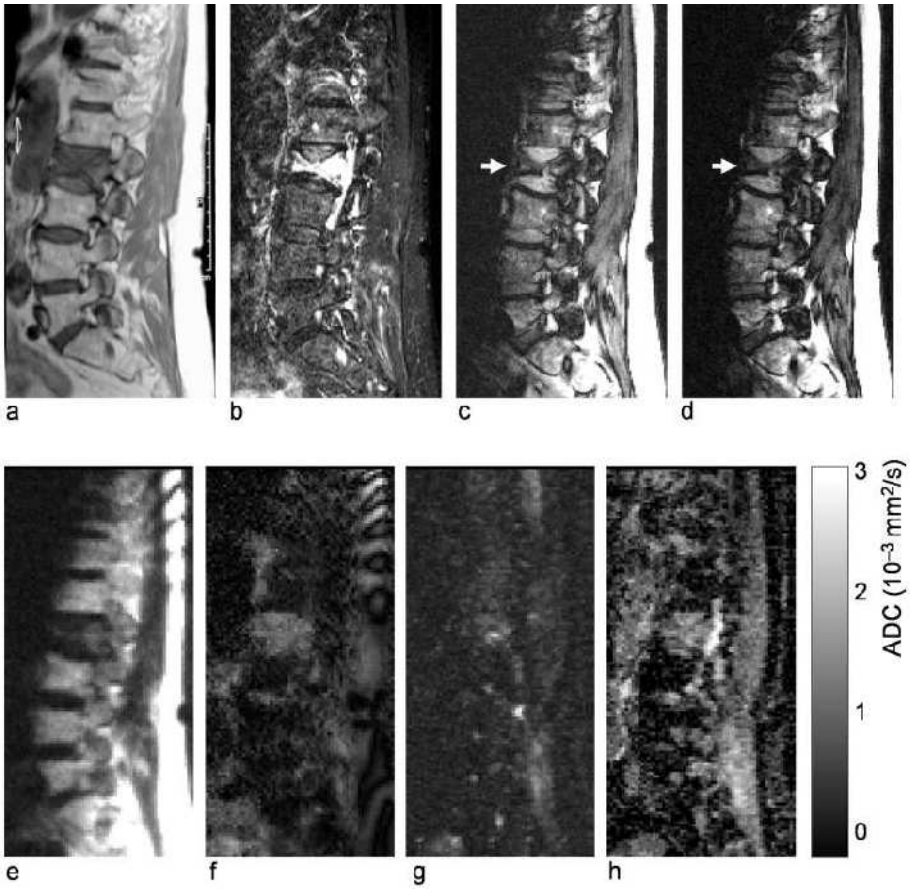

Figure 3: Example of a benign spontaneous osteoporotic vertebral compression fracture in a 75-year-old woman. (a) T1-weighted MRI shows hypointense fracture, (b) STIR acquisition shows hyperintense lesion. (c, d) Diffusion-weighted PSIF acquisitions with diffusion gradient moments of 69 and 138 ms mT/m, respectively. The lesion appears hypointense to isointense, indicating a benign fracture. (e) Diffusion-weighted single-shot TSE acquisition with b-value of 500 s/mm² and (f) corresponding ADC map with a diffusion coefficient in the lesion of 1.19×10^{-3} mm²/s. (g) Diffusion-weighted single-shot EPI acquisition with b-value of 500 s/mm²; note the artifacts and the low image quality. (h) Corresponding ADC map with a diffusion coefficient in the lesion of 1.51×10^{-3} mm²/s.

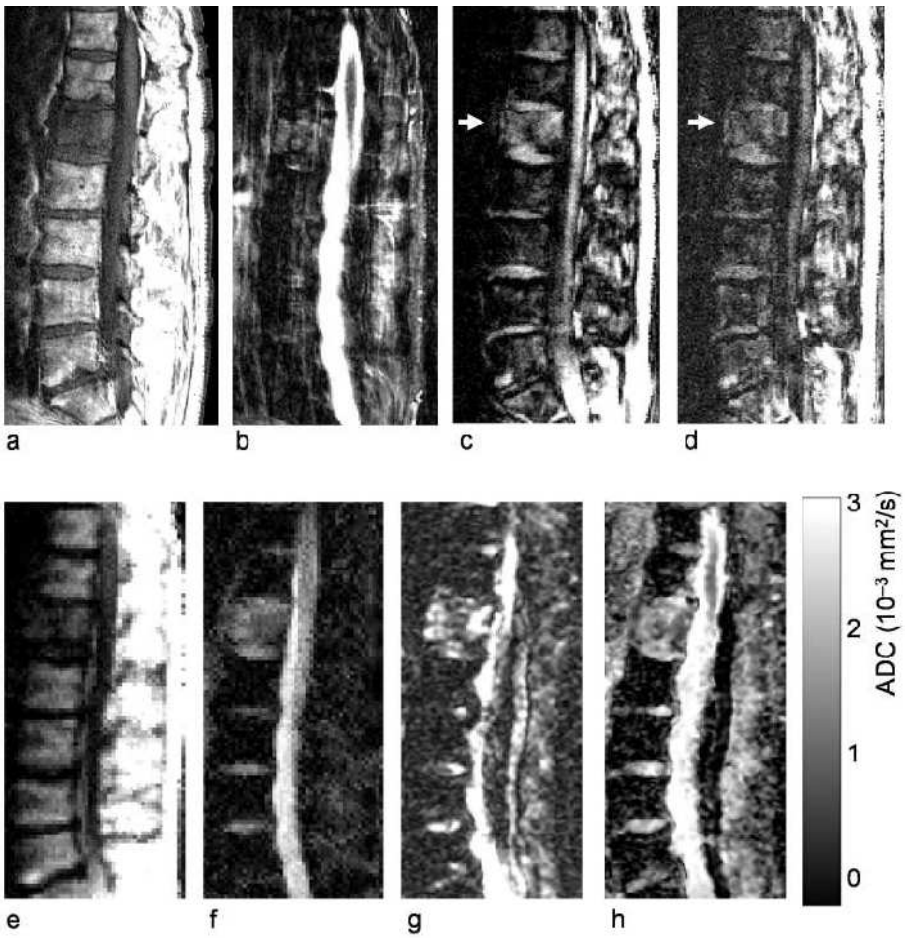

Figure 4: Example of a neoplastic vertebral compression fracture in a 72-year-old man with non-Hodgkin lymphoma. (a) T_1-weighted MRI shows hypointense fracture, (b) STIR acquisition shows hyperintense lesion despite some motion artifacts. (c, d) Diffusion-weighted PSIF acquisitions with diffusion gradient moments of 69 and 138 ms mT/m, respectively. The lesion appears hyperintense, indicating a malignant fracture. (e) Diffusion-weighted single-shot TSE acquisition with b-value of 500 s/mm² and (f) corresponding ADC map with a diffusion coefficient in the lesion of 1.05×10^{-3} mm²/s. (g) Diffusion-weighted single-shot EPI acquisition with b-value of 500 s/mm², (h) and corresponding ADC map with a diffusion coefficient in the lesion of 1.54×10^{-3} mm²/s.

Table 2: Quantitative DWI of normal and pathological vertebral bone marrow (v.b.m.)

Study	Pulse sequence[a]	b-values (s/mm²)	# of subjects	Apparent diffusion coefficient (10^{-3} mm²/s)			
				benign (osteoporotic/traumatic) fracture	malignant fracture (#) or metastasis (M)	inflammatory disease[b]	normal v.b.m.
Balliu et al. 2008[63]	ms-EPI	0, 500	45	1.90±0.39	0.92±0.13 (M)	0.96±0.49 (S)	–
Gašperšič et al. 2008[64]	ss-EPI	0, 400	30	–	–	≈1.3 (AS)	–
Sugimoto et al. 2008[65]	ss-EPI	0, 1000	25	–	–	–	≈0.2[c]
Byun et al. 2007[55]	ss-STE	0, 650	7	0.88±0.07	0.78±0.03 (#)	–	0.21±0.06
Tang et al. 2007[66]	ss-EPI	0, 300	34	2.23±0.21	1.04±0.03 (#)	–	–
Hatipoglu et al. 2007[67]	ss-EPI	0, 600	51	–	–	–	0.46±0.03[d]
Raya et al. 2007[68]	ss-FSE	0…750	32	1.25±0.26	0.97±0.14 (M)	1.48±0.33 (SD)	0.21±0.06
Oner et al. 2007[69]	ss-EPI	0, 600	24	1.61±0.46	0.72±0.31 (M)	1.51±0.25 (SD)	0.53±0.15
Oner et al. 2007[69]	ss-FSE	0, 600	24	1.54±0.36	0.69±0.30 (M)	1.21±0.24 (SD)	0.35±0.15
Griffith et al. 2006[70]	ss-EPI	0…500	103	–	–	–	0.46±0.08[e]
Pui et al. 2005[71]	ss-EPI	0…1000	51	–	1.02±0.36 (M)	1.15±0.42 (TB)	0.30±0.21
Yeung et al. 2004[52]	ss-EPI	0…500	44	–	–	–	0.44±0.11[f]
Ballon et al. 2004[72]	ss-EPI	0, 1000	1	–	0.70±0.21 (M)	–	–
Maeda et al. 2003[73]	LSDI	5, 1000	64	1.21±0.17	0.92±0.20 (#)[g]	–	–
Bammer et al. 2003[74]	LSDI	5, 650	15	1.02 – 1.97	–	–	0.23±0.08
Herneth et al. 2002[75]	ms-EPI	440, 880	22	1.61±0.37	0.71±0.27 (#)[h]	–	1.66±0.38
Byun et al. 2002[59]	ss-STE	0, 650	3	–	0.78±0.03 (M)	–	0.33±0.03
Chan et al. 2002[76]	ss-EPI	200…1000	32	1.94±0.35	0.82±0.20 (#)	0.98±0.21 (S)	0.23±0.05
Zhou et al. 2002[77]	ss-FSE	0, 150, 250	27	0.32±0.05	0.19±0.03 (M)	–	0.27 – 0.35
Dietrich et al. 2001[34]	rad-SE	50…350	6	–	–	–	0.33±0.06
Herneth et al. 2000[78]	ms-EPI	0, 440, 880	5	0.86	0.39±0.11 (M)	–	1.13±0.23
Typical values				**1.0 – 2.0**	**0.7 – 1.0**	**1.0 – 1.5**	**0.2 – 0.5**

[a] Sequences: ms-EPI: diffusion-weighted multi-shot (segmented) spin-echo echo-planar imaging sequence with fat saturation; ss-EPI: diffusion-weighted single-shot spin-echo echo-planar imaging sequence with fat saturation; ss-STE: diffusion-weighted single-shot stimulated-echo sequence; ss-FSE: diffusion-weighted single-shot fast-spin-echo sequence; LSDI: line-scan diffusion-weighted-imaging sequence; rad-SE: diffusion-weighted spin-echo sequence with radial readout
[b] S: spondylitis, AS: ankylosing spondylitis, SD: spondylodiskitis, TB: tuberculosis
[c] ADC of vertebrae fractured in follow-up: ≈0.6×10^{-3} mm²/s
[d] osteoporotic v.b.m.: (0.38±0.02)×10^{-3} mm²/s, osteopenic v.b.m.: (0.42±0.03)×10^{-3} mm²/s
[e] osteoporotic v.b.m.: (0.43±0.12)×10^{-3} mm²/s, osteopenic v.b.m.: (0.41±0.12)×10^{-3} mm²/s
[f] osteoporotic v.b.m.: (0.42±0.11)×10^{-3} mm²/s, osteopenic v.b.m.: (0.42±0.14)×10^{-3} mm²/s, normal v.b.m. in young healthy subjects: (0.50±0.09)×10^{-3} mm²/s
[g] non-collapsed metatstatic lesions: (0.83±0.17)×10^{-3} mm²/s
[h] non-collapsed metatstatic lesions: (0.69±0.24)×10^{-3} mm²/s

An alternative to non-quantitative diffusion-weighted SSFP imaging is the acquisition of diffusion-weighted images at two or more b-values in order to calculate the apparent diffusion coefficient as a quantitative measure of diffusion. Several studies applied quantitative DWI to normal and pathological vertebral bone marrow as summarized in Table 2. Although the displayed results exhibit a certain variability, there appear to be typical ADC ranges associated with normal and pathological vertebral bone marrow in the majority of these studies. Typical ADCs of normal vertebral bone marrow are relatively low between 0.2 and 0.5×10^{-3} mm²/s. Pathological bone marrow exhibits much higher diffusivities, ranging from about 0.7 to 1.0×10^{-3} mm²/s in metastases as well as malignant fractures, and from about 1.0 to 2.0×10^{-3} mm²/s in osteoporotic or traumatic fractures. Vertebrae affected by inflammatory disease such as spondylitis or tuberculosis have been reported with ADCs in an intermediate range from about 1.0 to 1.5×10^{-3} mm²/s. Although the measured ADC may be indicative for benign or malignant lesions, a considerable overlap has been described in several studies.

The general variability of the reported ADCs can be explained by the different pulse sequences and different diffusion weightings used in these studies. The most important difference with respect to the applied pulse sequences is the use of fat saturation, which is required for single-shot echo-planar imaging but is optional in combination with spin-echo or fast-spin-echo techniques. Since the ADC of vertebral fat is very close to zero, the calculated diffusion coefficients of normal bone marrow are systematically decreased when fat saturation is not applied. Typical values are in the range of 0.2 to 0.3×10^{-3} mm²/s, in contrast to 0.3 to 0.5×10^{-3}

mm^2/s with fat saturation. Smaller differences are seen in lesions, since the relative fat content is much lower there than in normal bone marrow. The chosen range of b-values can also systematically influence the measured ADCs: at very low b-values, the diffusion effect is known to be overestimated due to the contribution of perfusion to the signal attenuation[51,52], while the choice of relatively high b-values greater than about 600 s/mm^2 may result in an underestimation due to signal intensities comparable to the noise level.

The pathophysiological background of the described diffusion properties in vertebral bone marrow is not yet fully understood. Currently, the most probable hypothesis is that the molecular diffusion of water is substantially increased in osteoporotic fractures because of bone-marrow edema and the disruption of the trabecular structure. In malignant vertebral compression fractures, the diffusion is partially restricted due to the high cellularity of tumor tissue[16]. In DWI without fat suppression, the ratio of the fat and water contributions to the signal, i.e., the presence of red and yellow bone marrow or of tumor tissue, plays an important role as well. In particular in SSFP imaging, the signal is also influenced by in- and opposed-phase effects of the fat and water component, which depend on the interval between signal excitation and readout. Further studies are still required to understand the details of signal alterations in DWI of vertebral lesions.

Only very few studies examined DWI of the bone marrow outside of the vertebrae as listed in Table 3. The number of these studies is too small to establish typical ADC ranges for normal or pathological bone marrow in the examined regions. Only recently, these studies were complemented by whole-body applications of DWI based on a technique called diffusion-weighted whole-body imaging with background body-signal suppression (DWIBS) as suggested by Takahara et al.[13] The primary focus of these studies is the sensitive depiction of lesions rather than the quantification of their ADC. Although no ADCs were determined, it was demonstrated in several studies that whole-body DWI is very sensitive to bone-marrow lesions as well[14,53,54].

Conclusions

Diffusion-weighted imaging of the bone marrow requires considerably more robust imaging techniques than typical neurological DWI applications. Several different techniques and measurement parameters have been used for diffusion studies of bone marrow resulting in a relatively large variability of results. Although the optimization of the DWI technique is still a very active subject of research, the application of diffusion-weighted MRI in bone marrow is today an established examination technique that provides a unique contrast and that can help in the detection of bone-marrow pathologies and the differentiation of benign and malignant bone-marrow lesions. It has been applied particularly successful in DWI studies of vertebral lesions and of vertebral compression fractures.

Acknowledgements

This work was supported in part by the Deutsche Forschungsgemeinschaft (DFG), project number DI 1413/1-1.

Table 3: Quantitative DWI of non-vertebral bone marrow (b.m.)

Study	Pulse sequence[a]	b-values (s/mm^2)	# of subjects	Region/Pathology	Apparent diffusion coefficient (10^{-3} mm^2/s)	
					Pathology	Normal b.m.
Moon et al. 2007[79]	ss-EPI	0, 1000	13	Cranial b.m. metastases	0.90±0.25	–
Ragin et al. 2006[80]	ss-EPI	0, 1000	20	Cranial b.m./HIV patients	0.77 – 0.86	1.01 – 1.11
Nonomura et al. 2001[81]	ss-EPI	30, 300	37	Iliac b.m./malignant lymphoma	1.31±033[b]	0.83±0.71
Ballon et al. 2000[82]	ss-EPI	0, 1000	21	Iliac b.m./leukemia	0.48±0.13	0.53±0.07
Ward et al. 2000[83]	nav-SE	0, 980	50	Tibial b.m./bone bruise	0.40 – 1.30	0.10 – 0.25

[a] Sequences: ss-EPI: diffusion-weighted single-shot spin-echo echo-planar imaging sequence with fat saturation; nav-SE: diffusion-weighted spin-echo sequence with navigator-echo correction
[b] normal hypocellular iliac b.m.: $(0.36\pm0.31)\times10^{-3}$ mm^2/s

References

1. Karaarslan E, Arslan A. Diffusion weighted MR imaging in non-infarct lesions of the brain. Eur J Radiol 2008;65:402–416
2. Provenzale JM, Mukundan S, Barboriak DP. Diffusion-weighted and perfusion MR imaging for brain tumor characterization and assessment of treatment response. Radiology 2006;239:632–649
3. Cartes-Zumelzu FW, Stavrou I, Castillo M, Eisenhuber E, Knosp E, Thurnher MM. Diffusion-weighted imaging in the assessment of brain abscesses therapy. AJNR Am J Neuroradiol 2004;25:1310–1317
4. Horsfield MA, Jones DK. Applications of diffusion-weighted and diffusion tensor MRI to white matter diseases – a review. NMR Biomed. 2002;15:570–577
5. Schaefer PW, Copen WA, Lev MH, Gonzalez RG. Diffusion-weighted imaging in acute stroke. Magn Reson Imaging Clin N Am 2006;14:141–168
6. Davis DP, Robertson T, Imbesi SG. Diffusion-weighted magnetic resonance imaging versus computed tomography in the diagnosis of acute ischemic stroke. J Emerg Med 2006;31:269–277
7. Parikh T, Drew SJ, Lee VS, Wong S, Hecht EM, Babb JS, Taouli B. Focal liver lesion detection and characterization with diffusion-weighted MR imaging: comparison with standard breath-hold T2-weighted imaging. Radiology 2008;246:812–822
8. Zech CJ, Herrmann KA, Dietrich O, Horger W, Reiser MF, Schoenberg SO. Black-blood diffusion-weighted EPI acquisition of the liver with parallel imaging: comparison with a standard T2-weighted sequence for detection of focal liver lesions. Invest Radiol 2008;43:261–266
9. Zhang J, Tehrani YM, Wang L, Ishill NM, Schwartz LH, Hricak H. Renal masses: characterization with diffusion-weighted MR imaging--a preliminary experience. Radiology 2008;247:458–464
10. Cova M, Squillaci E, Stacul F, Manenti G, Gava S, Simonetti G, Pozzi-Mucelli R. Diffusion-weighted MRI in the evaluation of renal lesions: preliminary results. Br J Radiol 2004;77:851–857
11. Nagata S, Nishimura H, Uchida M, Sakoda J, Tonan T, Hiraoka K, Nagata K, Akiba J, Abe T, Hayabuchi N. Diffusion-weighted imaging of soft tissue tumors: usefulness of the apparent diffusion coefficient for differential diagnosis. Radiat Med 2008;26:287-295
12. Dietrich O, Raya JG, Sommer J, Deimling M, Reiser MF, Baur-Melnyk A. A comparative evaluation of a RARE-based single-shot pulse sequence for diffusion-weighted MRI of musculoskeletal soft-tissue tumors. Eur Radiol 2005;15:772–783
13. Takahara T, Imai Y, Yamashita T, Yasuda S, Nasu S, Van Cauteren M. Diffusion weighted whole body imaging with background body signal suppression (DWIBS): technical improvement using free breathing, STIR and high resolution 3D display. Radiat Med 2004;22:275–282
14. Kwee TC, Takahara T, Ochiai R, Nievelstein RA, Luijten PR. Diffusion-weighted whole-body imaging with background body signal suppression (DWIBS): features and potential applications in oncology. Eur Radiol 2008;18:1937–1952
15. Raya JG, Dietrich O, Reiser MF, Baur-Melnyk A. Methods and applications of diffusion imaging of vertebral bone marrow. J Magn Reson Imaging 2006;24:1207–1220
16. Baur A, Stäbler A, Brüning R, Bartl R, Krödel A, Reiser M, Deimling M. Diffusion-weighted MR imaging of bone marrow: differentiation of benign versus pathologic compression fractures. Radiology 1998;207:349–356
17. Karchevsky M, Babb JS, Schweitzer ME. Can diffusion-weighted imaging be used to differentiate benign from pathologic fractures? A meta-analysis. Skeletal Radiol 2008;37:791–795
18. Raya JG, Dietrich O, Reiser MF, Baur-Melnyk A. Techniques for diffusion-weighted imaging of bone marrow. Eur J Radiol 2005;55:64–73
19. Hahn EL. Spin echoes. Phys Rev 1950;80:580–594
20. Stejskal EO, Tanner JE. Spin diffusion measurements: spin echoes in the presence of a time-dependent field gradient. J Chem Phys 1965;42:288–292
21. Xing D, Papadakis NG, Huang CL, Lee VM, Carpenter TA, Hall LD. Optimised diffusion-weighting for measurement of apparent diffusion coefficient (ADC) in human brain. Magn Reson Imaging 1997;15:771–784
22. Trouard TP, Sabharwal Y, Altbach MI, Gmitro AF. Analysis and comparison of motion-correction techniques in diffusion-weighted imaging. J Magn Reson Imaging 1996;6:925–935
23. Norris DG. Implications of bulk motion for diffusion-weighted imaging experiments: effects, mechanisms, and solutions. J Magn Reson Imaging 2001;13:486–495
24. Basser PJ, Mattiello J, LeBihan D. MR diffusion tensor spectroscopy and imaging. Biophys J 1994;66:259-267
25. Basser PJ, Pierpaoli C. Microstructural and physiological features of tissues elucidated by quantitative-diffusion-tensor MRI. J Magn Reson B 1996;111:209–119
26. Basser PJ, Pierpaoli C. A simplified method to measure the diffusion tensor from seven MR images. Magn Reson Med 1998;39:928–934
27. Merboldt KD, Hanicke W, Frahm J. Self-diffusion NMR imaging using stimulated echoes. J Magn Reson 1985;64:479–486
28. Taylor DG, Bushell MC. The spatial mapping of translational diffusion coefficients by the NMR imaging technique. Phys Med Biol 1985;30:345–349
29. Le Bihan D, Breton E, Lallemand D, Grenier P, Cabanis E, Laval-Jeantet M. MR imaging of intravoxel incoherent motions: application to diffusion and perfusion in neurologic disorders. Radiology 1986;161:401–407
30. Ordidge RJ, Helpern JA, Qing ZX, Knight RA, Nagesh V. Correction of motional artifacts in diffusion-weighted MR images using navigator echoes. Magn Reson Imaging 1994;12:455–460
31. Anderson AW, Gore JC. Analysis and correction of motion artifacts in diffusion weighted imaging. Magn Reson Med 1994;32:379–387
32. Dietrich O, Heiland S, Benner T, Sartor K. Reducing motion artefacts in diffusion-weighted MRI of the brain: efficacy of navigator echo correction and pulse triggering. Neuroradiology 2000;42:85–91
33. Gmitro AF, Alexander AL. Use of a projection reconstruction method to decrease motion sensitivity in diffusion-weighted MRI. Magn Reson Med. 1993;29:835–838
34. Dietrich O, Herlihy A, Dannels WR, Fiebach J, Heiland S, Hajnal JV, Sartor K. Diffusion-weighted imaging of the spine using radial k-space trajectories. MAGMA Magn Reson Mater Phy 2001;12:23–31
35. Gudbjartsson H, Maier SE, Mulkern RV, Mórocz IA, Patz S, Jolesz FA. Line scan diffusion imaging. Magn Reson Med 1996;36:509–519

36. Turner R, Le Bihan D, Maier J, Vavrek R, Hedges LK, Pekar J. Echo-planar imaging of intravoxel incoherent motion. Radiology 1990;177:407–414

37. Jaermann T, Pruessmann KP, Valavanis A, Kollias S, Boesiger P. Influence of SENSE on image properties in high-resolution single-shot echo-planar DTI. Magn Reson Med 2006;55:335–342

38. Norris DG, Börnert P, Reese T, Leibfritz D. On the application of ultra-fast RARE experiments. Magn Reson Med 1992;27:142–164

39. Schick F. SPLICE: sub-second diffusion-sensitive MR imaging using a modified fast spin-echo acquisition mode. Magn Reson Med 1997;38:638–644

40. Alsop DC. Phase insensitive preparation of single-shot RARE: application to diffusion imaging in humans. Magn Reson Med 1997;38:527–533

41. Pipe JG, Farthing VG, Forbes KP. Multishot diffusion-weighted FSE using PROPELLER MRI. Magn Reson Med 2002;47:42–52 (erratum in: Magn Reson Med 2002;47:621)

42. Gyngell ML. The application of steady-state free precession in rapid 2DFT NMR imaging: FAST and CE-FAST sequences. Magn Reson Imaging 1988;6:415–419

43. Bruder H, Fischer H, Graumann R, Deimling M. A new steady-state imaging sequence for simultaneous acquisition of two MR images with clearly different contrasts. Magn Reson Med 1988;7:35–42

44. Le Bihan D. Intravoxel incoherent motion imaging using steady-state free precession. Magn Reson Med 1988;7:346–351

45. Merboldt KD, Bruhn H, Frahm J, Gyngell ML, Hänicke W, Deimling M. MRI of "diffusion" in the human brain: new results using a modified CE-FAST sequence. Magn Reson Med 1989;9:423–429

46. Kaiser R, Bartholdi E, Ernst RR. Diffusion and field-gradient effects in NMR Fourier spectroscopy. J Chem Phys 1974;60:2966–2979

47. Wu EX, Buxton RB. Effect of diffusion on the steady-state magnetization with pulsed field gradients. J Magn Reson 1990;90:243–253

48. Miller KL, Hargreaves BA, Gold GE, Pauly JM. Steady-state diffusion-weighted imaging of in vivo knee cartilage. Magn Reson Med 2004;51:394–398

49. Castillo M, Arbelaez A, Smith JK, Fisher LL. Diffusion-weighted MR imaging offers no advantage over routine noncontrast MR imaging in the detection of vertebral metastases. AJNR Am J Neuroradiol 2000;21:948–953

50. Hackländer T, Scharwächter C, Golz R, Mertens H. Value of diffusion-weighted imaging for diagnosing vertebral metastases due to prostate cancer in comparison to other primary tumors. Rofo Fortschr Röntgenstr 2006;178:416–424

51. Le Bihan D, Breton E, Lallemand D, Aubin ML, Vignaud J, Laval-Jeantet M. Separation of diffusion and perfusion in intravoxel incoherent motion MR imaging. Radiology 1988;168:497–505

52. Yeung DK, Wong SY, Griffith JF, Lau EM. Bone marrow diffusion in osteoporosis: evaluation with quantitative MR diffusion imaging. J Magn Reson Imaging 2004;19:222–228

53. Mürtz P, Krautmacher C, Träber F, Gieseke J, Schild HH, Willinek WA. Diffusion-weighted whole-body MR imaging with background body signal suppression: a feasibility study at 3.0 Tesla. Eur Radiol 2007;17:3031–3037

54. Koh DM, Takahara T, Imai Y, Collins DJ. Practical aspects of assessing tumors using clinical diffusion-weighted imaging in the body. Magn Reson Med Sci 2007;6:211–224

55. Byun WM, Jang HW, Kim SW, Jang SH, Ahn SH, Ahn MW. Diffusion-weighted magnetic resonance imaging of sacral insufficiency fractures: comparison with metastases of the sacrum. Spine 2007;32:E820–E824

56. Park SW, Lee JH, Ehara S, Park YB, Sung SO, Choi JA, Joo YE. Single shot fast spin echo diffusion-weighted MR imaging of the spine; Is it useful in differentiating malignant metastatic tumor infiltration from benign fracture edema? Clin Imaging 2004;28:102–108

57. Abanoz R, Hakyemez B, Parlak M. Diffusion-weighted imaging of acute vertebral compression: Differential diagnosis of benign versus malignant pathologic fractures. Tani Girisim Radyol 2003;9:176–183

58. Baur A, Huber A, Dürr HR, Nikolaou K, Stäbler A, Deimling M, Reiser M. Differentiation of benign osteoporotic and neoplastic vertebral compression fractures with a diffusion-weighted, steady-state free precession sequence. Rofo Fortschr Röntgenstr 2002;174:70–75

59. Byun WM, Shin SO, Chang Y, Lee SJ, Finsterbusch J, Frahm J. Diffusion-weighted MR imaging of metastatic disease of the spine: assessment of response to therapy. AJNR Am J Neuroradiol 2002;23:906–912

60. Yasumoto M, Nonomura Y, Yoshimura R, Haraguchi K, Ito S, Ohashi I, Shibuya H. MR detection of iliac bone marrow involvement by malignant lymphoma with various MR sequences including diffusion-weighted echo-planar imaging. Skeletal Radiol 2002;31:263–269

61. Spuentrup E, Buecker A, Adam G, van Vaals JJ, Guenther RW. Diffusion-weighted MR imaging for differentiation of benign fracture edema and tumor infiltration of the vertebral body. AJR Am J Roentgenol 2001;176:351–358

62. Baur A, Huber A, Ertl-Wagner B, Dürr R, Zysk S, Arbogast S, Deimling M, Reiser M. Diagnostic value of increased diffusion weighting of a steady-state free precession sequence for differentiating acute benign osteoporotic fractures from pathologic vertebral compression fractures. AJNR Am J Neuroradiol 2001;22:366–372

63. Balliu E, Vilanova JC, Peláez I, Puig J, Remollo S, Barceló C, Barceló J, Pedraza S. Diagnostic value of apparent diffusion coefficients to differentiate benign from malignant vertebral bone marrow lesions. Eur J Radiol 2008 (epub ahead of print)

64. Gaspersic N, Sersa I, Jevtic V, Tomsic M, Praprotnik S. Monitoring ankylosing spondylitis therapy by dynamic contrast-enhanced and diffusion-weighted magnetic resonance imaging. Skeletal Radiol 2008;37:123–131

65. Sugimoto T, Tanigawa N, Ikeda K, Ohmura N, Maehara M, Kariya S, Kojima H, Komemushi A, Ha-Kawa SK, Saito Y, Tajika A, Kinoshita T, Sawada S. Diffusion-weighted imaging for predicting new compression fractures following percutaneous vertebroplasty. Acta Radiol 2008;49:419–426

66. Tang G, Liu Y, Li W, Yao J, Li B, Li P. Optimization of b value in diffusion-weighted MRI for the differential diagnosis of benign and malignant vertebral fractures. Skeletal Radiol 2007;36:1035–1041

67. Hatipoglu HG, Selvi A, Ciliz D, Yuksel E. Quantitative and diffusion MR imaging as a new method to assess osteoporosis. AJNR Am J Neuroradiol 2007;28:1934–1937

68. Raya JG, Dietrich O, Birkenmaier C, Sommer J, Reiser MF, Baur-Melnyk A. Feasibility of a RARE-based sequence for

quantitative diffusion-weighted MRI of the spine. Eur Radiol 2007;17:2872–2879

69. Oner AY, Tali T, Celikyay F, Celik A, Le Roux P. Diffusion-weighted imaging of the spine with a non-carr-purcell-meiboom-gill single-shot fast spin-echo sequence: initial experience. AJNR Am J Neuroradiol 2007;28:575–580
70. Griffith JF, Yeung DK, Antonio GE, Wong SY, Kwok TC, Woo J, Leung PC. Vertebral marrow fat content and diffusion and perfusion indexes in women with varying bone density: MR evaluation. Radiology 2006;241:831–838
71. Pui MH, Mitha A, Rae WI, Corr P. Diffusion-weighted magnetic resonance imaging of spinal infection and malignancy. J Neuroimaging 2005;15:164–170
72. Ballon D, Watts R, Dyke JP, Lis E, Morris MJ, Scher HI, Uluğ AM, Jakubowski AA. Imaging therapeutic response in human bone marrow using rapid whole-body MRI. Magn Reson Med 2004;52:1234–1238
73. Maeda M, Sakuma H, Maier SE, Takeda K. Quantitative assessment of diffusion abnormalities in benign and malignant vertebral compression fractures by line scan diffusion-weighted imaging. AJR Am J Roentgenol 2003;181:1203–1209
74. Bammer R, Herneth AM, Maier SE, Butts K, Prokesch RW, Do HM, Atlas SW, Moseley ME. Line scan diffusion imaging of the spine. AJNR Am J Neuroradiol 2003;24:5–12
75. Herneth AM, Philipp MO, Naude J, Funovics M, Beichel RR, Bammer R, Imhof H. Vertebral metastases: assessment with apparent diffusion coefficient. Radiology 2002;225:889–894
76. Chan JH, Peh WC, Tsui EY, Chau LF, Cheung KK, Chan KB, Yuen MK, Wong ET, Wong KP. Acute vertebral body compression fractures: discrimination between benign and malignant causes using apparent diffusion coefficients. Br J Radiol 2002;75:207–214
77. Zhou XJ, Leeds NE, McKinnon GC, Kumar AJ. Characterization of benign and metastatic vertebral compression fractures with quantitative diffusion MR imaging. AJNR Am J Neuroradiol 2002;23:165–170
78. Herneth AM, Naude J, Philipp M, Beichel R, Trattnig S, Imhof H. The value of diffusion-weighted MRT in assessing the bone marrow changes in vertebral metastases. Radiologe 2000;40:731–736
79. Moon WJ, Lee MH, Chung EC. Diffusion-weighted imaging with sensitivity encoding (SENSE) for detecting cranial bone marrow metastases: comparison with T1-weighted images. Korean J Radiol 2007;8:185–191
80. Ragin AB, Wu Y, Storey P, Cohen BA, Edelman RR, Epstein LG, Gartner S. Bone marrow diffusion measures correlate with dementia severity in HIV patients. AJNR Am J Neuroradiol 2006;27:589–592
81. Nonomura Y, Yasumoto M, Yoshimura R, Haraguchi K, Ito S, Akashi T, Ohashi I. Relationship between bone marrow cellularity and apparent diffusion coefficient. J Magn Reson Imaging 2001;13:757–760
82. Ballon D, Dyke J, Schwartz LH, Lis E, Schneider E, Lauto A, Jakubowski AA. Bone marrow segmentation in leukemia using diffusion and T (2) weighted echo planar magnetic resonance imaging. NMR Biomed 2000;13:321–328
83. Ward R, Caruthers S, Yablon C, Blake M, DiMasi M, Eustace S. Analysis of diffusion changes in posttraumatic bone marrow using navigator-corrected diffusion gradients. AJR Am J Roentgenol 2000;174:731–734